PHYSICAL REVIEW MATERIALS **7**, 114402 (2023)

Comparative study of the magnetism in Mn_3RhGe and related compound Mn_3IrSi

Amelia E. Hall,[1] Pascal Manuel,[2] Dmitry D. Khalyavin,[2] Fabio Orlandi,[2] Daniel A. Mayoh,[1] Lieh-Jeng Chang,[3] Yu-Sheng Chen,[3] David G. C. Jonas,[1] Martin R. Lees,[1] and Geetha Balakrishnan[1,*]

[1] *Department of Physics, University of Warwick, Coventry CV4 7AL, United Kingdom*
[2] *ISIS Facility, Rutherford Appleton Laboratory, Harwell, Oxford, Didcot OX11 0QX, United Kingdom*
[3] *Department of Physics, National Cheng Kung University, No. 1 University Road, Tainan 70101, Taiwan*

(Received 20 January 2023; revised 29 September 2023; accepted 3 October 2023; published 3 November 2023)

The Mn_3XY (X = Co, Rh, Ir and Y = Si, Ge) family of materials adopts an ordered form of the chiral β-Mn structure lacking inversion symmetry. Polycrystalline samples of Mn_3IrSi and a new member in this family, Mn_3RhGe, have been synthesized and investigated with heat capacity, magnetic susceptibility, and neutron powder diffraction measurements. Mn_3RhGe and Mn_3IrSi exhibit long-range magnetic order below 225(2) and 230(2) K, respectively. The neutron diffraction data reveal a high-temperature incommensurate magnetic structure in Mn_3RhGe, which transitions into a noncollinear commensurate antiferromagnetic ground state upon cooling via a phase coexistence in a wide temperature range. The presence of the incommensurate magnetic order reveals a significant role of exchange interactions beyond nearest and next-nearest neighbors. Mn_3IrSi shares the noncollinear commensurate magnetic structure for all temperatures and shows no evidence of incommensurate magnetism.

DOI: 10.1103/PhysRevMaterials.7.114402

I. INTRODUCTION

Materials such as the Co-Zn-Mn alloys adopt the β-Mn structure with the $P4_132$ space group and are capable of hosting skyrmions at temperatures up to, and even higher than, room temperature [1]. Skyrmions are novel magnetic vortices which are topologically protected and robust, and thus of interest for potential future device applications [2]. There are different mechanisms for the formation of skyrmions. In the case of the Co-Zn-Mn alloys, they are thought to emerge from a competition between the antisymmetric Dzyaloshinskii-Moriya interaction [3,4] and the symmetric ferromagnetic exchange interaction.

The Mn_3XY family of materials, where X = Co, Rh, Ir and Y = Si, Ge, take an ordered form of the β-Mn structure with the $P2_13$ space group. The Mn atoms occupy the $12b$ Wyckoff position and form a trillium lattice [5], i.e., a lattice of three-dimensional corner-sharing triangles (see Fig. 1). Similar to the parent β-Mn structure, the lattice can be considered as geometrically frustrated; however, the lower symmetry of the ordered structure implies three distinct nearest-neighbor $12b$-$12b$ Wyckoff position exchange interactions instead of only two different nearest-neighbor $12d$-$12d$ interactions for the parent $P4_132$ structure.

Despite the similarities in the structures of the Co-Zn-Mn alloys and the Mn_3XY family of materials, the latter are found to display very different magnetic behaviors. Mn_3CoGe, Mn_3IrSi, and Mn_3IrGe have been previously investigated using powder neutron diffraction and have been found to share very similar noncollinear antiferromagnetic orderings [6–9]. Therefore, it is clear that if skyrmions are exhibited by these ternary materials, they must arise from mechanisms different from those in the Co-Zn-Mn alloys and are perhaps more similar to those at play in Gd_2PdSi_3 [10] and $Gd_3Ru_4Al_{12}$ [11].

Mn_3IrSi has been reported to order antiferromagnetically below $T_N = 225$ K. The Mn atoms carry a magnetic moment of 2.97(4) μ_B [6], with angles close to 120° between them, Mn_3IrGe shares this type of magnetic structure, with a study of a series of solid solutions of $Mn_3Ir(Si_{1-x}Ge_x)$ finding a linear increase in the unit-cell volume with increasing Ge content, but no change in the nature of the noncollinear antiferromagnetic ordering or the transition temperature, $T_N = 225(10)$ K [9]. The ordered moments in Mn_3IrGe were found to be 3.39(4) μ_B/Mn, larger than those seen in Mn_3IrSi despite their similar critical temperatures. A more recent study has been successful in growing single crystals of Mn_3IrSi and reports a large hump below $T_N = 230$ K, which may indicate either the presence of a spin density wave or the opening of an antiferromagnetic gap at the Fermi surface [12]. An additional anomaly at 100 K was also observed in the magnetic susceptibility and requires further investigation.

A study of the solid solution $Mn_3Ir_{1-y}Co_ySi$ found that the nearly 120° antiferromagnetic structure was present for compositions with $y \leqslant 0.2$, while unidentified short-range magnetic orderings were observed for $y = 0.8-1.0$. Mn_3CoSi has been studied using neutron diffraction [7] and

---

[*] g.balakrishnan@warwick.ac.uk

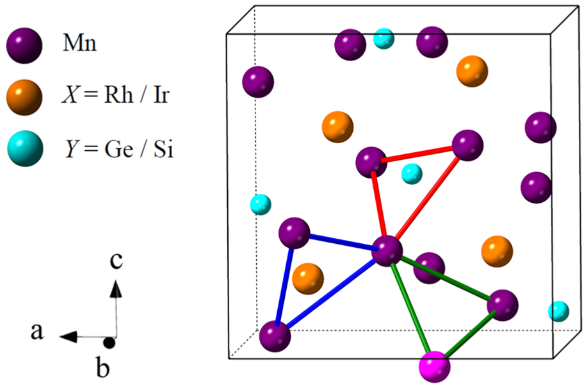

FIG. 1. Nuclear structure for the Mn_3XY family in the $P2_13$ space group. Selected corner-sharing triangles formed by Mn atoms occupying the $12b$ lattice positions are shown, with equivalent bonds marked in the same color and a Mn atom lying outside the unit cell illustrated in pink. In the related $P4_132$ space group, the bonds marked in blue and red are equivalent, resulting in a reduction from three to two in the number of different nearest-neighbor interactions.

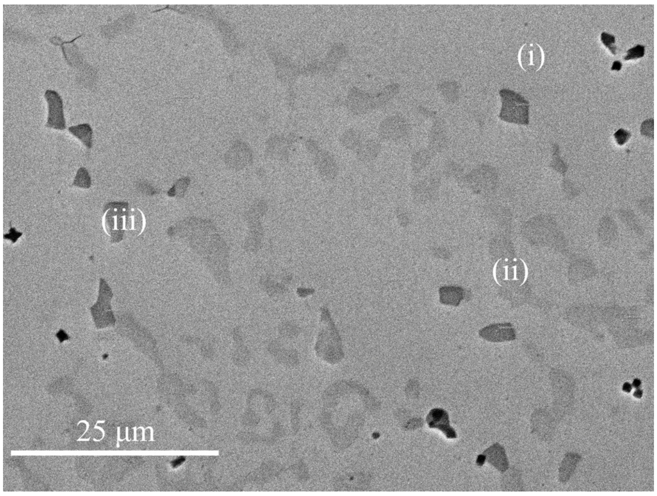

FIG. 2. Scanning electron microscope image of a metallographic slide of Mn_3RhGe with three areas of differing contrast marked as (i), (ii), and (iii).

linear-muffin-tin orbital calculations [13] to find no long-range ordering stabilized in the material. A recent study on Mn_3RhSi found evidence for short-range spin correlations resulting in a strong diffuse scattering, which persists to high temperatures well above the long-range ordering temperature $T_N = 190$ K [14]. The magnetic ordering for this compound is found to be similar to other members of the family with close to 120° spin configuration in the triangular units.

Here, we report on the successful synthesis of Mn_3RhGe and perform a detailed comparison of this material with the related compound Mn_3IrSi. Heat capacity measurements show the presence of a transition to a long-range magnetically ordered state in Mn_3RhGe at 240(5) K. In addition, our high-resolution powder neutron diffraction data reveal that Mn_3RhGe displays an incommensurate magnetic phase before adopting a noncollinear commensurate ground state. In contrast, detailed neutron diffraction data for Mn_3IrSi, used to fully explore how the magnetism of this material evolves with temperature, show no evidence for incommensurate magnetism.

II. EXPERIMENTAL DETAILS

Polycrystalline samples of Mn_3RhGe and Mn_3IrSi were synthesized using argon arc melting. Pieces of high-purity Mn, Ir, and Si, or Mn, Rh, and Ge, were melted together in stoichiometric quantities to obtain buttons of the polycrystalline material. The as-cast samples were used for the study.

To confirm the successful preparation of Mn_3RhGe, energy-dispersive x-ray (EDX) analysis on selected samples was performed with a ZEISS GeminiSEM 500 scanning electron microscope (SEM) operating at 20 kV. The typical average composition of the as-cast ingots, determined from 16 spectra collected on each ingot, was found to be $Mn_{2.99(10)}Rh_{0.827(2)}Ge_{1.18(10)}$. This is close to the desired stoichiometry, with just a slight rhodium deficiency. The variation in composition across the bulk sample was found to be small (see Supplemental Material [15] for details on the compositional analysis of both Mn_3RhGe and Mn_3IrSi).

A metallographic slide of Mn_3RhGe was prepared by mounting a sample in conductive plastic and polishing it to an optical finish. This slide was analyzed using EDX. An SEM image of the slide is displayed in Fig. 2. Areas of different contrast confirm the presence of a main phase, (i) $Mn_{3.105(10)}Rh_{0.89(3)}Ge_{1.00(4)}$, as well as two minor impurity phases: (ii) $Mn_{3.019(8)}Rh_{0.58(3)}Ge_{1.39(2)}$, and (iii) $Mn_{2.902(12)}Rh_{0.122(13)}Ge_{0.975(10)}$ or, approximately, Mn_3Ge, with the small amounts of detected Rh likely due to sampling of the sample around the pockets of Mn_3Ge, due to their small size. The average results from several spectra are tabulated in Table I. Mn_3Ge orders antiferromagnetically with a small ferromagnetic component at a transition temperature T_N of approximately 370 K [16]. These phases make up a small volume of the sample and both heat capacity and powder neutron diffraction data suggest that the minority phases do not affect the magnetic ordering observed in the bulk of the sample (see Sec. III).

Heat capacity measurements were performed using a Quantum Design Physical Property Measurement System (PPMS) with Apiezon N grease used to ensure good thermal contact between the sample and the sample stage. The 2τ thermal relaxation method was used and our materials were

TABLE I. Average composition from energy-dispersive x-ray spectra of the Mn_3RhGe sample. The regions (i)–(iii), sampled for the metallographic slide of this sample, are indicated in Fig. 2.

	Mn (%)	Rh (%)	Ge (%)
Polycrystalline button			
	59(1)	17(1)	24(1)
Metallographic slide			
(i)	62.1(2)	20.1(8)	17.8(6)
(ii)	60.5(6)	11.8(6)	27.7(6)
(iii)	72.6(6)	3(1)	24.4(6)

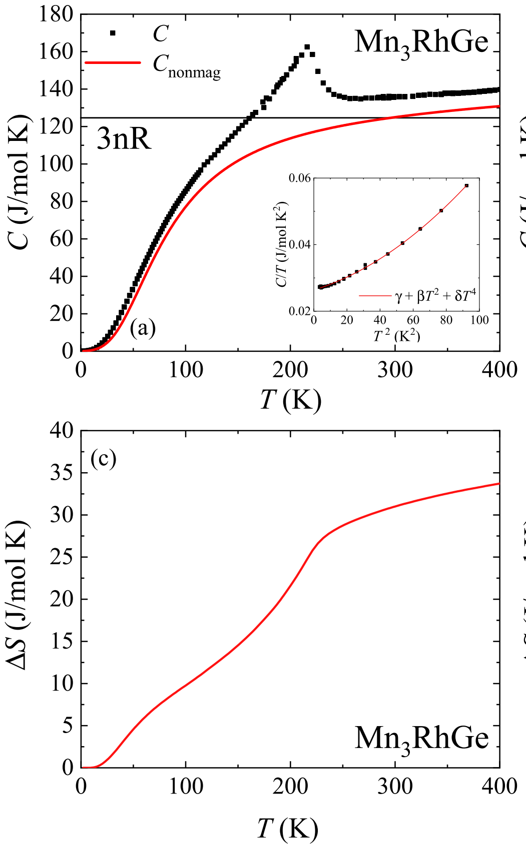

FIG. 3. Heat capacity vs temperature in zero magnetic field for (a) Mn_3RhGe and (b) Mn_3IrSi. The change in magnetic entropy for (c) Mn_3RhGe and (d) Mn_3IrSi.

measured at temperatures from 1.8 to 400 K in zero applied field.

Powder neutron diffraction measurements on Mn_3RhGe and Mn_3IrSi were performed using the WISH instrument at the ISIS neutron source [17]. The large number of position-sensitive detectors and solid methane moderator provide a wide accessible d-spacing range with a good resolution, making it ideal for these measurements. The powdered samples were mounted inside a 3-mm-diameter vanadium canister and the neutron diffraction data were taken in zero field for a range of temperatures between 1.5 and 300 K for Mn_3RhGe and 5 and 300 K for Mn_3IrSi. The data were analyzed using the FULLPROF software suite [18] and JANA2020 [19] against the data measured in detector banks at average 2θ values of 58°, 90°, 122°, and 152.8°, each covering 32° of the scattering plane.

III. RESULTS AND DISCUSSION

A. Heat capacity

Heat capacity versus temperature data for Mn_3RhGe and Mn_3IrSi are shown in Figs. 3(a) and 3(b), respectively. Mn_3RhGe shows a single clear anomaly indicative of a magnetic transition with the midpoint of the transition at 225(5) K, while Mn_3IrSi exhibits a two-step anomaly with an onset at around 230(2) K, providing strong evidence for long-range magnetic ordering. These transition temperatures agree well with those observed in χ_{dc} versus T data for each material (see Supplemental Material [15]) and with the literature [12], although there is no evidence for a two-step transition in either the dc susceptibility data for Mn_3IrSi or previous studies. The origin of this behavior is unclear. One possibility is a small variation in the composition of the Mn_3IrSi across the measured sample. No further transitions are observed in $C(T)$ for either compound over the studied temperature range.

At low temperatures, the data can be fit using $C(T)/T = \gamma + \beta T^2 + \delta T^4$, where γ is the electronic contribution to the heat capacity and the βT^2 and δT^4 terms arise from the phonons. The Debye temperature is given by $\Theta_D = \sqrt[3]{\frac{12}{5}\frac{nR\pi^4}{\beta}}$, where $n = 5$ is the number of atoms per formula unit and R is the molar gas constant. Fitting the low-temperature data gives $\gamma = 2.64(1) \times 10^{-2}$ and $2.92(1) \times 10^{-2}$ J/mol K^2, and $\Theta_D = 398(4)$ and 450(4) K, for Mn_3RhGe and Mn_3IrSi, respectively. The γ for Mn_3IrSi is slightly higher than the $\gamma = 2.3 \times 10^{-2}$ J/mol K^2 recorded in a previous study [12].

In order to estimate the magnetic entropy, the nonmagnetic contribution to the heat capacity at high temperature, $C_{nonmag} = C_{electronic} + C_{phonon}$, was evaluated, where $C_{electronic} = \gamma T$ and C_{phonon} was determined using the Debye model. The Debye temperatures that were used are $\Theta_D = 340(40)$ K for Mn_3RhGe, and $\Theta_D = 400(30)$ K for Mn_3IrSi. These are a little below those calculated from the low-temperature fits to give an upper limit on the phonon contribution. Around 300 K, C_{nonmag} exceeds the $15R$ from

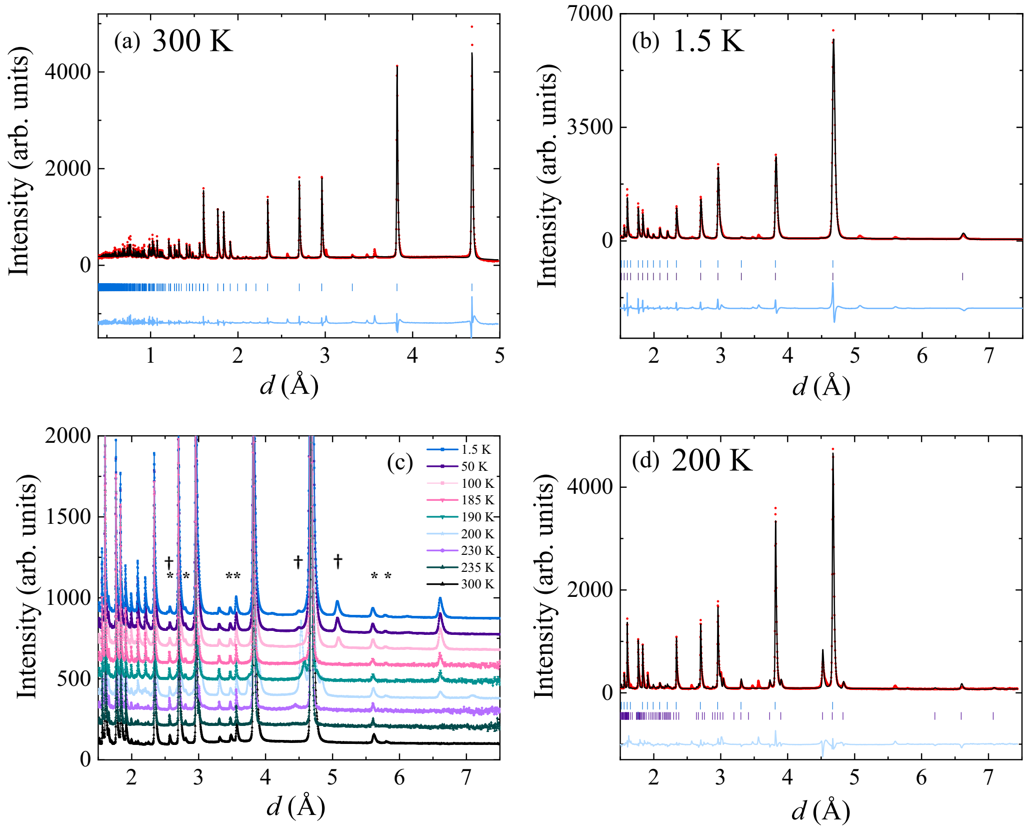

FIG. 4. Powder neutron diffraction data and Rietveld refinements for Mn_3RhGe of (a) the nuclear structure at 300 K (detector bank with the average $2\theta = 152.8^\circ$) and (b) the nuclear and magnetic structures at 1.5 K (detector bank with the average $2\theta = 90.0^\circ$). The observed, calculated, and difference patterns are marked in red, black, and blue, respectively. Nuclear and magnetic Bragg peaks are marked with blue and purple "|" tick marks, respectively. (c) Evolution of the powder neutron diffraction profiles for Mn_3RhGe with temperature from 1.5 to 300 K (detector bank with the average $2\theta = 90.0^\circ$). Each profile is offset by 150 arbitrary units for clarity. Peaks marked with an asterisk are due to unidentified impurity phases, likely the Rh-deficient phase seen in the SEM/EDX measurements. The peaks observed below 150 K marked with a dagger are due to a small amount (weight fraction 0.2%) of the magnetic impurity MnO [20–22]. The data at 185, 190, 230, and 230 K were taken in the single-frame experimental setup, while the rest of the data were taken in the double-frame regime. The fit to the nuclear and magnetic structures at (d) 200 K (detector bank with the average $2\theta = 90.0^\circ$), showing the incommensurate magnetic peaks, is displayed with the same key as (a) and (b).

the Dulong-Petit law due to the γT contribution. The nonmagnetic contribution was then removed and the change in magnetic entropy over the magnetic transition was estimated by integrating $\Delta C(T)/T$ with respect to temperature, where $\Delta C(T) = C(T) - C_{\mathrm{nonmag}}(T)$. At 300 K, this gave a ΔS of 33(5) and 37(5) J/mol K, for Mn_3RhGe and Mn_3IrSi, respectively. These results are close to the expected value for Mn^{4+}, $\Delta S = 34.6$ J/mol K.

B. Powder neutron diffraction

1. Mn_3RhGe

The nuclear structure of Mn_3RhGe was refined from the powder neutron diffraction data collected at 300 K [see Fig. 4(a)]. A structural model with the cubic $P2_13$ space group and the unit-cell parameter $a = 6.62104(9)$ Å provided a satisfactory fitting quality and the obtained structural parameters are summarized in Table II. Several small impurity peaks were observed in the data that could not be accounted for by the model. We failed to index these peaks using a commensurate or single incommensurate propagation vector, making a scenario of lower symmetry very unlikely. Apparently these reflections belong to the Rh-deficient phase detected in the metallographic slide discussed above or to some other small impurity phase.

Cooling the sample down to 1.5 K resulted in the appearance of additional reflections in the diffraction pattern [Fig. 4(b)], confirming the presence of long-range magnetic order. The magnetic reflections could be indexed with $\mathbf{k_0} = (0, 0, 0)$ propagation vector, indicating that the magnetic unit cell is identical to the nuclear one. To model the magnetic scattering, we adopted the method based on space-group representation theory implemented in the FULLPROF package [18]. The best refinement quality was found using the one-dimensional $m\Gamma_1$ irreducible representation of the paramagnetic $P2_13$ space group [Fig. 4(b)]. This representation enters three times into the decomposition of the magnetic reducible representation associated with the Mn 12*b* Wyckoff position, yielding three orthogonal basis functions. The atomic components of these basis functions are listed in Table III, along with the corresponding mixing coefficients obtained in the refinement procedure. The refined size of the

TABLE II. Atomic coordinates and components of the Mn magnetic moments, M_i, ($i = x, y, z$), for Mn_3RhGe extracted from refinements of powder neutron diffraction data collected at 300, 200, and 1.5 K (detector banks with an average 2θ of 152.8°, 90.0°, and 152.8°), respectively. In the case of the incommensurate magnetic structure (200 K), the modulation function of the Mn magnetic moments is given by the Fourier series, $M_{i,j,l} = \sum_{n=1}^{\infty} A_{i,j}^{n} \sin(2\pi n[\mathbf{r}_{j,l}\mathbf{k}_1]) + B_{i,j}^{n} \cos(2\pi n[\mathbf{r}_{j,l}\mathbf{k}_1])$, where $\mathbf{r}_{j,l}$ indicates position of the jth atom of the average structure in the lth unit cell. In our refinement, only the Fourier coefficients for the first harmonic ($n = 1$), A_i^1 and B_i^1, were refined.

	300 K			$P2_13$	
$R_p = 6.69\%$		$R_{wp} = 6.81\%$		$a = 6.62104(9)$ Å	
	Wyck.	x	y	z	B_{iso} (Å^2)
Mn	$12b$	0.117(2)	0.2017(10)	0.4572(11)	1.37(10)
Rh	$4a$	0.6861(9)	0.6861(9)	0.6861(9)	1.5(3)
Ge	$4a$	0.0636(6)	0.0636(6)	0.0636(6)	0.91(12)
	200 K			$P2_12_12_1.1'(0, 0, \gamma)000s$	
$R_p = 7.55\%$		$R_{wp} = 7.69\%$		$a, b, c = 6.6106(1)$ Å	
	Wyck.	x	y	z	B_{iso} (Å^2)
Mn1	$4a$	0.606(2)	0.7043(15)	0.960(2)	0.000(12)
A_i^1		1.24(6)	−0.08(11)	1.32(6)	
B_i^1		−1.11(8)	−1.05(12)	0.97(10)	
Mn2	$4a$	0.540(2)	0.3938(15)	0.204(2)	0.086(14)
A_i^1		−1.20(7)	−1.17(11)	0.7(2)	
B_i^1		−1.29(9)	0.7(2)	−1.0(2)	
Mn3	$4a$	0.296(2)	0.4598(15)	0.894(2)	0.01(2)
A_i^1		−1.20(8)	0.90(10)	1.00(12)	
B_i^1		1.32(8)	1.07(12)	0.63(13)	
Rh	$4a$	0.0612(9)	0.9388(9)	0.4388(9)	0.037(4)
Ge	$4a$	0.6829(11)	0.3171(11)	0.8171(11)	0.010(3)
	1.5 K			$P2_13.1$	
$R_p = 7.01\%$		$R_{wp} = 7.28\%$		$a = 6.60100(5)$ Å	
	Wyck.	x	y	z	B_{iso} (Å^2)
Mn	$12b$	0.120(2)	0.2060(14)	0.452(2)	1.05(9)
M_i		1.34(2)	2.2(2)	−1.84(14)	
Rh	$4a$	0.6862(11)	0.6862(11)	0.6862(11)	1.4(3)
Ge	$4a$	0.0640(8)	0.0640(8)	0.0640(8)	0.36(14)

magnetic moments is found to be 3.07(1) μ_B/Mn, with a noncollinear magnetic structure (Fig. 5), revealing the presence of competing interactions. This is quite natural, taking into account that the nearest-neighbor Mn-Mn exchange interactions form a three-dimensional network of corner-sharing triangular units. The one-dimensional nature of the mΓ_1

TABLE III. Atomic components of the basis vectors, Ψ_i, localized on the $12b$ Wyckoff position of the $P2_13$ space group and transformed by the $m\Gamma_1$ irreducible representation. Magnetic structure is presented as a linear combination of these basis vectors with the mixing coefficients c_i ($\sum_i c_i\Psi_i$) obtained in refinements performed using the Wish detector bank with the average $2\theta = 58°$. The 12 Mn sites in the $12b$ Wyckoff position are Mn1(x, y, z), Mn2($-x + 1/2, -y, z + 1/2$), Mn3($-x, y + 1/2, -z + 1/2$), Mn4($x + 1/2, -y + 1/2, -z$), Mn5(z, x, y), Mn6($z + 1/2, -x_1/2, -y$), Mn7($-z + 1/2, -x, y + 1/2$), Mn8($-z, x + 1/2, -y + 1/2$), Mn9(y, z, x), Mn10($-y, z + 1/2, -x + 1/2$), Mn11($y + 1/2, -z + 1/2, -x$), and Mn12($-y + 1/2, -z, x + 1/2$).

	Basis vectors											
	Mn1	Mn2	Mn3	Mn4	Mn5	Mn6	Mn7	Mn8	Mn9	Mn10	Mn11	Mn12
mΓ_1												
Ψ_1	(1,0,0)	$(\bar{1}, 0, 0)$	$(\bar{1}, 0, 0)$	(1,0,0)	(0,1,0)	$(0, \bar{1}, 0)$	$(0, \bar{1}, 0)$	(0,1,0)	(0,0,1)	$(0, 0, \bar{1})$	$(0, 0, \bar{1})$	(0,0,1)
Ψ_2	(0,1,0)	$(0, \bar{1}, 0)$	(0,1,0)	$(0, \bar{1}, 0)$	(0,0,1)	$(0, 0, \bar{1})$	(0,0,1)	(0,0,1)	(1,0,0)	$(\bar{1}, 0, 0)$	(1,0,0)	$(\bar{1}, 0, 0)$
Ψ_3	(0,0,1)	(0,0,1)	$(0, 0, \bar{1})$	$(0, 0, \bar{1})$	(1,0,0)	(1,0,0)	$(\bar{1}, 0, 0)$	$(\bar{1}, 0, 0)$	(0,1,0)	(0,1,0)	$(0, \bar{1}, 0)$	$(0, \bar{1}, 0)$

Mixing coefficients				
Compound	c_1	c_2	c_3	R_{Mag}
Mn_3RhGe	1.34(2)	2.2(2)	−1.84(14)	5.93%
Mn_3IrSi	1.51(2)	1.8(3)	−1.8(2)	2.35%

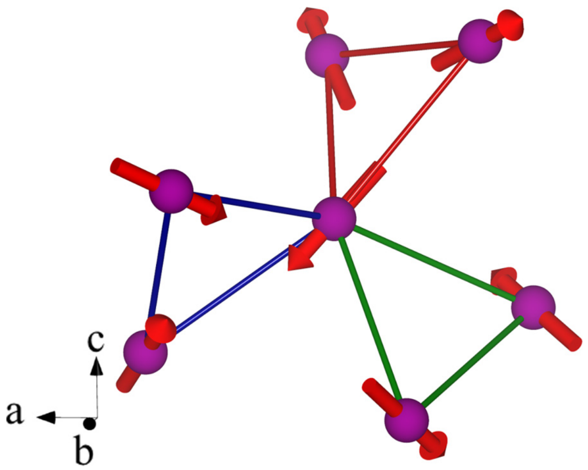

FIG. 5. Mn atoms in Mn_3RhGe are shown with the magnetic moments (red arrows) to display the ground-state magnetic structure. A similar magnetic structure for Mn_3IrSi is displayed in the Supplemental Material [15].

representation implies that the cubic symmetry is preserved in the magnetically ordered state. Moreover, since this representation is a branch of the totally symmetric representation of the nonmagnetic $P2_13$ space group, the corresponding magnetic symmetry is $P2_13.1$ [23]. A similar noncollinear cubic magnetic ground state has also been found in the isostructural Mn_3IrSi, Mn_3CoGe, and Mn_3IrSi compounds [6–9], revealing its universal character. A description of the magnetic structure in this space group is provided in Table II.

The evolution of the diffraction patterns for Mn_3RhGe with temperature is displayed in Fig. 4(c). No obvious indication of the existence of short-range ordering, such as a broadening of the magnetic peaks, is observed at any temperatures for this material. Surprisingly, however, warming the sample up to 175 K resulted in the appearance of a new set of reflections with a concomitant decrease of the $\mathbf{k_0} = 0$ magnetic peaks [Fig. 6(a)]. This was unexpected since no visible anomaly has been detected in either the magnetic susceptibility or the specific heat below 240 K.

The new magnetic reflections could not be indexed with a commensurate cell and required the use of incommensurate propagation vector $\mathbf{k_1} = (0, 0, \gamma)$, with γ strongly dependent on temperature [Fig. 6(c), inset]. The intensity of these reflections increased with temperature to a maximum at 195 K, where the $\mathbf{k_0} = 0$ magnetic phase practically vanished [Figs. 6(b) and 6(c)]. This behavior indicates that the commensurate and the incommensurate magnetic phases coexist over a wide temperature range. This can explain why there is no visible second anomaly in the susceptibility and specific heat data below 240 K. Warming the sample above 225 K resulted in the loss of long-range magnetic order, but clear diffuse scattering was observed even at higher temperatures, indicating the presence of short-range spin correlations well above the transition temperature. To efficiently exploit symmetry constraints, the refinement of the incommensurate magnetic structure was approached using the superspace formalism [24]. The relevant magnetic superspace groups were generated by the ISODISTORT software [25,26] and tested versus the experimental data using the JANA2020 program [19]. The best fit to the data was found in the $P2_12_12_1.1'(0, 0, \gamma)000s$ superspace group associated with the $m\Delta_1$ irreducible representation of $P2_13$ [see Fig. 4(d)]. The refinement was performed assuming only the incommensurate magnetic phase; however, the presence of a small amount

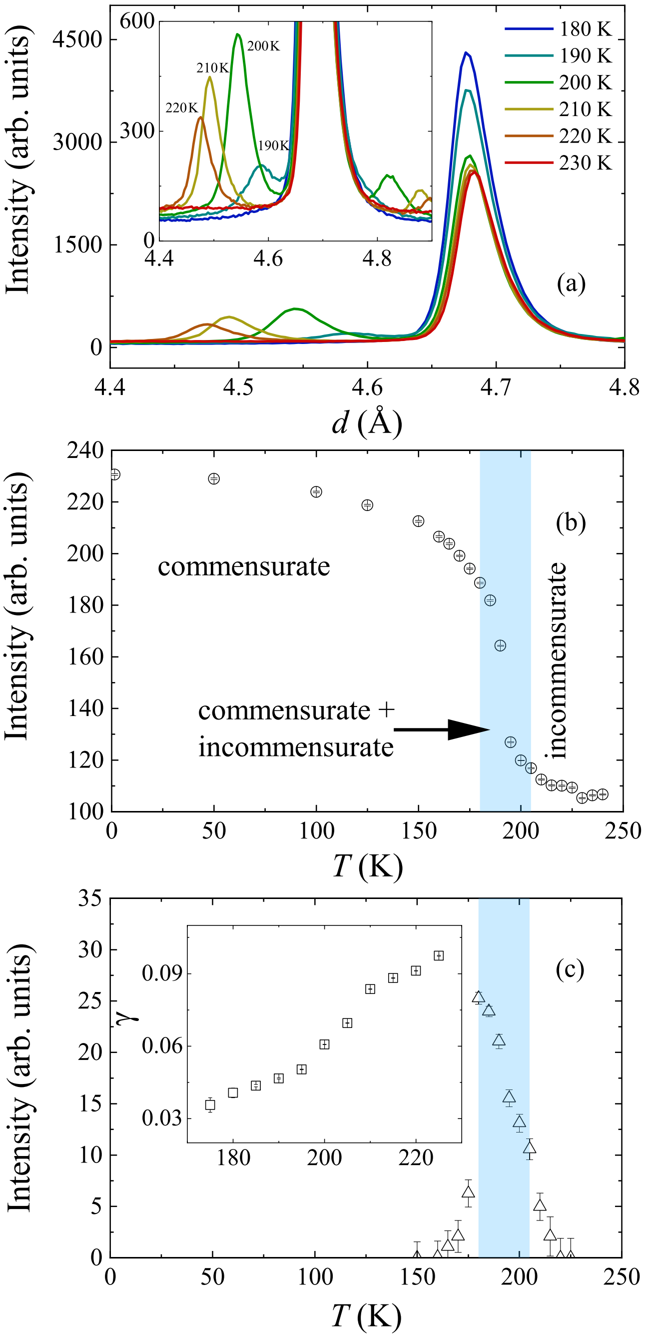

FIG. 6. (a) Portion of neutron diffraction pattern for Mn_3RhGe in the vicinity of the (110) reflection with a strong magnetic contribution from the commensurate $\mathbf{k_0} = 0$ phase, which is transferred to magnetic satellites above 175 K. Inset: Temperature dependence of the magnetic satellites in more detail. (b) Integrated intensities of the (110) reflection and (c) the magnetic satellite to the left of this reflection as a function of temperature. Inset: Temperature dependence of the incommensurate propagation vector.

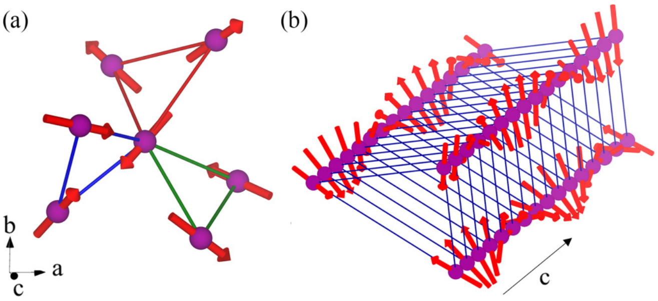

FIG. 7. Structure of the incommensurate magnetic phase found in Mn_3RhGe at 200 K showing (a) the configuration of three different Mn-Mn nearest-neighbor interactions in the $P2_12_12_1.1'(0,0,\gamma)000s$ space group and (b) a single triangle of Mn atoms extended along the c direction to better show the evolution of the incommensurate winding.

(a few percent) of the low-temperature $\mathbf{k_0} = 0$ phase could not be excluded. This phase scatters on top of the strong nuclear reflections and therefore its reliable refinement was not possible due to correlations with the structural parameters. In order to reduce the number of variables present for the incommensurate magnetic structure, the refinement was constrained so that the moments were equal across all Mn atoms and of constant size. Initially, the moments were set to a reasonable value of 2 μ_B/Mn, as expected for the temperature, and were then varied within the constant moment constraint. As a result, a final refined moment of 1.8(2) μ_B/Mn is extracted from the data at 200 K, and the atomic parameters and modulation functions are listed in Table II, along with the equivalent information at 300 and 1.5 K.

In common with the commensurate ground state, the high-temperature incommensurate magnetic structure implies a noncollinear arrangement of the nearest-neighbor Mn spins in the triangular units (see Fig. 7 and Supplemental Material [15]). Upon propagation through the crystal, the spins gradually rotate, forming an incommensurate structure, which preserves the relative angles between the moments in the triangles. Taking into account the small component of the propagation vector [$k_z = 0.0663(1)$ at 200 K], the incommensurate structure is therefore only a small perturbation of the low-temperature ground state.

The observation of the higher-temperature magnetic phase in Mn_3RhGe naturally gives rise to the question of whether this incommensurate spin order can be associated with the noncentrosymmetric crystal structure of the Mn_3XY family of materials, and if so, whether other members of the family might also exhibit this phase. To answer these questions, the magnetic ordering in the related compound Mn_3IrSi was revisited through a detailed high-resolution neutron powder diffraction study reported below.

2. Mn_3IrSi

Powder neutron diffraction data for Mn_3IrSi are shown in Fig. 8. The structural parameters obtained at 300 K in the cubic $P2_13$ space group are summarized in Table IV and the fitting quality is shown in Fig. 8(a). The unit-cell parameter at this temperature is found to be $a = 6.50407(7)$ Å. Several small impurity peaks were observed in the powder profile that could not be indexed by the cubic cell. They were excluded from the refinement procedure. It should also be pointed out that the Ir-containing sample is highly absorbing, and the points at which the intensity of the calculated fit does not fully capture the intensity of the observed data can be attributed to this. Despite this, the Bragg R-factor for this fit was $R_{\mathrm{Bragg}} = 6.459\%$, which indicates good agreement between the calculated fit and observed data. The commensurate magnetic structure of Mn_3IrSi, refined from the data collected at 5 K [see Fig. 8(b)], as well as its refined moment size [2.92(1) μ_B/Mn], agrees well with the published literature [6,8] and is very similar to the $\mathbf{k_0}$ magnetic structure found for Mn_3RhGe (see Tables III and IV and the Supplemental Material [15]).

The diffraction patterns for Mn_3IrSi as they evolve with temperature are displayed in Fig. 8(c). Magnetic peaks begin to appear at temperatures in line with the transition temperatures extracted from our heat capacity and dc susceptibility data, $T_N = 230(2)$ K. Unlike Mn_3RhGe, there is no evidence of any incommensurate magnetic phase in Mn_3IrSi, which appears to enter its commensurate ground state immediately at

TABLE IV. Atomic coordinates and components of the Mn magnetic moments, M_i, ($i = x, y, z$), for Mn_3IrSi extracted from refinements of powder neutron diffraction data collected at 300 and 5 K performed for detector banks with average $2\theta = 152.8^\circ$ and 58°, respectively.

	300 K			$P2_13$	
	$R_p = 7.34\%$	$R_{wp} = 7.61\%$		$a = 6.50407(7)$ Å	
	Wyck.	x	y	z	B_{iso} (Å^2)
Mn	12b	0.1179(13)	0.2073(8)	0.4549(7)	1.02(9)
Ir	4a	0.6831(3)	0.6831(3)	0.6831(3)	0.55(6)
Si	4a	0.0662(8)	0.0662(8)	0.0662(8)	0.3(2)
	5 K			$P2_13.1$	
	$R_p = 6.96\%$	$R_{wp} = 7.11\%$		$a = 6.49081(7)$ Å	
	Wyck.	x	y	z	B_{iso} (Å^2)
Mn	12b	0.1187(14)	0.2074(10)	0.4544(8)	0.55(10)
M_i		1.51(2)	1.8(3)	−1.8(2)	
Ir	4a	0.6829(4)	0.6829(4)	0.6829(4)	0.18(6)
Si	4a	0.066(1)	0.066(1)	0.066(1)	0.4(2)

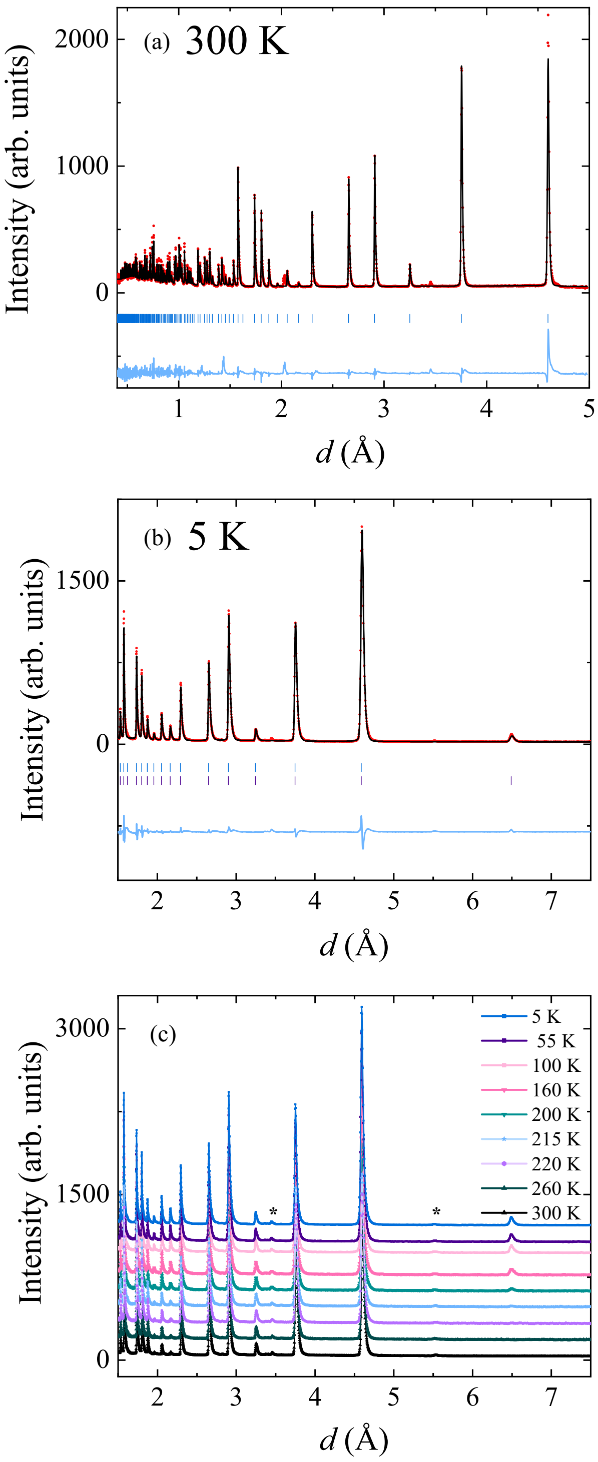

FIG. 8. Powder neutron diffraction data and Rietveld refinements for Mn_3IrSi of (a) the nuclear structure at 300 K (bank at $2\theta = 152.8^\circ$) and (b) the nuclear and magnetic structure at 5 K (bank at $2\theta = 90.0^\circ$). The observed, calculated, and difference patterns are marked in red, black, and blue, respectively. Nuclear and magnetic Bragg peaks are marked with blue and purple "|" tick marks, respectively. (c) Evolution of the neutron diffraction profiles for Mn_3IrSi with temperature from 5 to 300 K (bank at $2\theta = 90.0^\circ$). Each profile is offset by 150 arbitrary units for clarity. Peaks marked with an asterisk are due to an unidentified impurity phase.

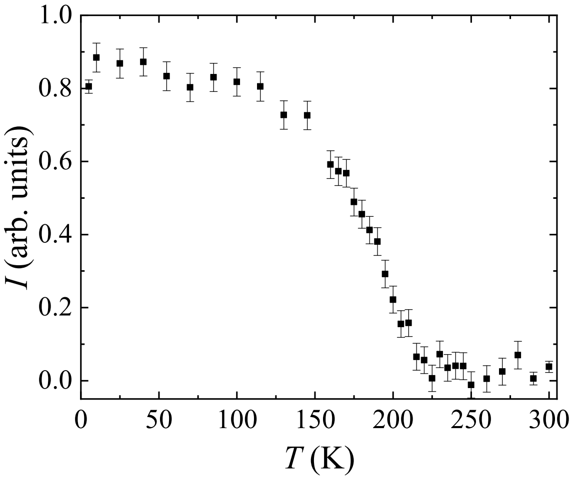

FIG. 9. Integrated intensity I of the (001) peak as a function of temperature for Mn_3IrSi, taken on warming from 5 to 300 K.

230 K. The temperature resolution of the data, collected in 5 K steps, combined with the high resolution of WISH makes the possibility of missing an incommensurate phase unlikely. The integrated intensity of the (001) magnetic peak as a function of temperature is displayed in Fig. 9. No changes in the magnetic structure below T_N can be concluded based on this plot and therefore the origin of the two-step transition seen in the heat capacity of this material is not clear from the neutron data and merits further investigation.

The absence of incommensurate magnetic order in Mn_3IrSi strongly indicates that this phase is not directly related to the noncentrosymmetric nature of the Mn_3XY compounds and the associated Dzyaloshinkii-Moriya interactions. This conclusion is further supported by the symmetry of the commensurate ground state transformed by the $m\Gamma_1$ irreducible representation of the $P2_13$ space group. The antisymmetrized square of this representation does not contain vector representation, which implies that the Lifshitz invariant [27] is not allowed in the Landau free-energy decomposition. This type of free-energy invariant promotes incommensurate states through antisymmetric exchange and is often responsible for long-period modulations in weakly anisotropic magnetic systems with noncentrosymmetric crystal structures, such as $Cr_{1/3}NbS_2$ [28] and MnSi [29]. The incommensurate magnetic phase in Mn_3RhGe, therefore, appears to be a result of a delicate balance between the competing symmetric exchange interactions imposed by the frustrated triangular based topology.

To verify this conclusion, we undertook mean-field calculations for Heisenberg spins taking into account the couplings between nearest-neighbor Mn as well as the interactions beyond them. The approach is similar to the theoretical study of the β-Mn frustrated lattice by Canals and Lacroix [30]. The interesting result of Canals and Lacroix's calculation is the presence of the lowest-energy modes which are dispersionless along the (γ, γ, γ) line of symmetry. This indicates that no long-range magnetic order is possible if one considers only the nearest-neighbor interactions. The ordered structure of

Mn_3RhGe is less symmetric and implies three nonequivalent nearest-neighbor interactions, in comparison with only two in β-Mn. However, keeping them antiferromagnetic, it is not possible to remove the ground-state degeneracy and the lowest-energy modes stay dispersionless [see Fig. 10(a)]. The experimentally determined magnetic ground state of Mn_3RhGe and Mn_3IrSi, as well as other members of the family such as Mn_3IrGe, Mn_3CoGe, and Mn_3CoSi [6–9], implies antiferromagnetic character for the nearest-neighbor interactions in Mn_3XY and a strong competition between them. We therefore chose the idealized case of the frustrated lattice, when $J_1 = J_2 = J_3 = -1$, to qualitatively investigate the relevant interactions stabilizing the experimentally observed magnetic structures. Although in the real systems these interactions are slightly different, it does not change the conclusions made for the most frustrated case with equal J_1, J_2, and J_3.

The interactions beyond the nearest neighbor are defined in the Supplemental Material [15], along with the corresponding Mn-Mn distances. In the range between 3 and 4 Å, there is only one interaction, denoted as J_4 (where the Mn-Mn distance is 3.4 Å), and in the range between 4 and 5 Å, one can identify eight additional couplings, $J_5 - J_{12}$. The ground-state degeneracy was found to be unstable when the next-nearest-neighbor interaction is included and a finite positive J_4 removes the degeneracy and selects a $\mathbf{k} = 0$ ordered state [Fig. 10(b)]. Apparently, this is the case of the ground state of Mn_3RhGe and Mn_3IrSi, as well as many other members of the family. By systematic exploration of the phase space formed by the third and higher-order interactions, $J_5 - J_{12}$, we have found that a small positive J_6 shifts the energy minimum from the $\mathbf{k} = 0$ to an incommensurate propagation vector along the $(0, 0, \gamma)$, line of symmetry [Fig. 10(c)]. For instance, keeping the nearest-neighbor interactions antiferromagnetic and equivalent, $J_1 = J_2 = J_3 = -1$, and taking $J_4 = 0.3$ to be ferromagnetic, the experimentally observed propagation vector $\mathbf{k} = (\sim 0.07, 0, 0)$ at $T = 200$ K is selected at $J_6 = 0.11$.

The propagation vector was found to be very sensitive to the magnitude of J_6, whose slight temperature variation can explain the change of the magnetic structure and the significant temperature dependence of γ. Increasing this interaction from 0.11 to 0.12 results in a change of γ from 0.07 to 0.12, while values below 0.1 do not perturb the commensurate $\mathbf{k} = 0$ ordered state. Thus, the presence of the incommensurate magnetic order in Mn_3RhGe signifies the relevance of the ferromagnetic interactions beyond the nearest- and next-nearest neighbor. This conclusion is fully consistent with the study of spin correlations in a closely related Co-doped β-Mn system by Paddison *et al.* [31]. This study revealed the presence of prominent ferromagnetic further-neighbor interactions and found that the ferromagnetic correlations between fifth-nearest neighbors were as strong as nearest-neighbor antiferromagnetic correlations.

IV. SUMMARY

A new member of the Mn_3XY family of materials, Mn_3RhGe, with the ordered β-Mn crystal structure, has been found to exhibit a transition to a magnetically ordered state at 225(2) K. The magnetic structure is incommensurate with orthorhombic $P2_12_12_1.1'(0, 0, \gamma)000s$ symmetry, where γ increases from ~0.03 to ~0.1 between 175 and 225 K. At lower temperatures, the magnetic order transforms into a commensurate ground state with the $\mathbf{k_0} = (0, 0, 0)$ propagation vector and cubic $P2_13.1$ magnetic symmetry. The transformation takes place via a phase coexistence in the temperature range of $175 \leqslant T \leqslant 200$ K. The magnetic moments in the commensurate phase are ordered into a noncollinear pattern with a close to 120° configuration in the triangular units formed by nearest-neighbor exchange interactions with a magnetic moment of size 3.07(1) μ_B/Mn at 1.5 K. In contrast, Mn_3IrSi exhibits only the cubic noncollinear magnetic order, with a refined moment size of 2.92(1) μ_B/Mn, and no evidence of the incommensurate magnetism has been found. The refined moment sizes for both materials are consistent with the moment size expected for Mn^{4+}, in agreement with the magnetic entropy from heat capacity measurements.

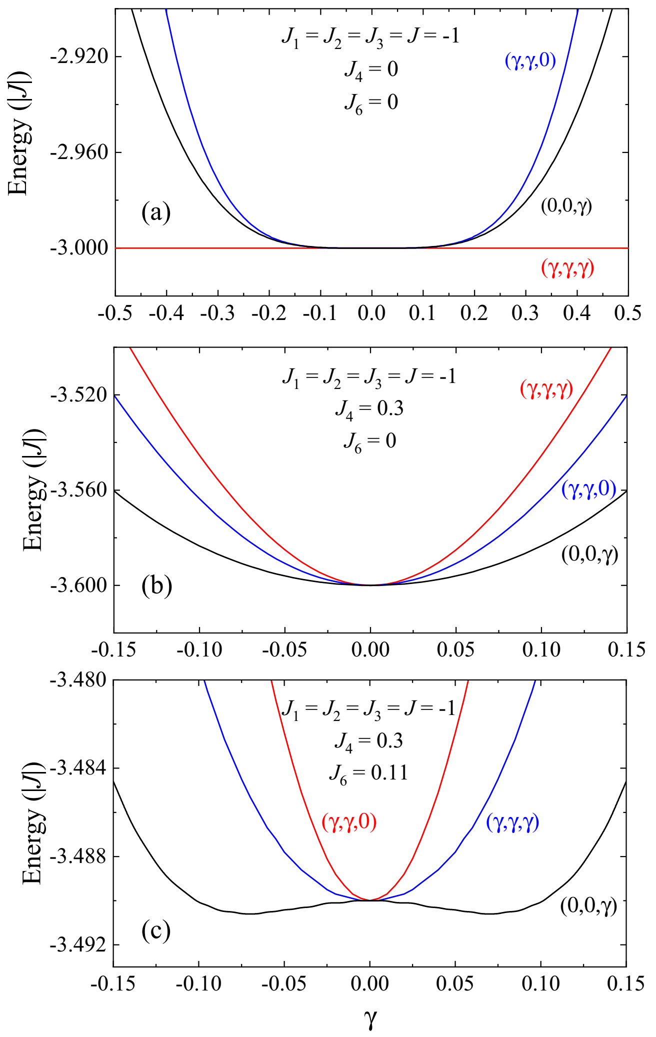

FIG. 10. Dispersion curves of the lowest eigenvalues along different lines of symmetry for different sets of the exchange interactions. The set of J values shown in (c) reproduces the propagation vector in the incommensurate magnetic phase of Mn_3RhGe, observed at 200 K.

This study indicates that the modulated structure in Mn_3RhGe is stabilized by the frustrated symmetric Heisenberg interactions, rather than a competition between symmetric and antisymmetric exchange associated with the noncentrosymmetric nature of the ordered β-Mn crystal structure. With this in mind, the presence of an incommensurate magnetic phase in Mn_3RhGe, and the absence of a similar phase in the Ir compound, can perhaps be related to differences between the 4*d* element Rh and the 5*d* element Ir. This incommensurate phase in the Rh compound is especially interesting with regards to its potential for hosting novel magnetic phenomena, such as skyrmions, and highlights that the Mn_3XY family and β-Mn structure-type materials are interesting candidates for further study.

ACKNOWLEDGMENTS

This work was financially supported by the EPSRC (Grants No. EP/N032128/1 and No. EP/W00562X/1). We would like to acknowledge the technical support provided by Thomas Orton, Patrick Ruddy, and Ryan Williams, without whom many of these measurements would not have been possible. This work was supported by UKRI and STFC through the provision of beam time at the ISIS Neutron and Muon Source [32].

[1] Y. Tokunaga, X. Z. Yu, J. S. White, H. M. Rønnow, D. Morikawa, Y. Taguchi, and Y. Tokura, Nat. Commun. **6**, 7638 (2015).
[2] S. Seki and M. Mochizuki, *Skyrmions in Magnetic Materials* (Springer International, New York, 2016).
[3] I. Dzyaloshinsky, J. Phys. Chem. Solids **4**, 241 (1958).
[4] T. Moriya, Phys. Rev. **120**, 91 (1960).
[5] J. M. Hopkinson and H.-Y. Kee, Phys. Rev. B **74**, 224441 (2006).
[6] T. Eriksson, R. Lizárraga, S. Felton, L. Bergqvist, Y. Andersson, P. Nordblad, and O. Eriksson, Phys. Rev. B **69**, 054422 (2004).
[7] T. Eriksson, L. Bergqvist, Y. Andersson, P. Nordblad, and O. Eriksson, Phys. Rev. B **72**, 144427 (2005).
[8] T. Eriksson, S. Felton, R. Lizárraga, O. Eriksson, P. Nordblad, and Y. Andersson, J. Magn. Magn. Mater. **272-276**, 823 (2004).
[9] T. Eriksson, L. Berbqvist, O. Nordblad, O. Eriksson, and Y. Andersson, J. Solid State Chem. **177**, 4058 (2004).
[10] T. Kurumaji, T. Nakajima, M. Hirschberger, A. Kikkawa, Y. Yamasaki, H. Sagayama, H. Nakao, Y. Taguchi, T.-H. Arima, and Y. Tokura, Science **365**, 914 (2019).
[11] M. Hirschberger, T. Nakajima, S. Gao, L. Peng, A. Kikkawa, T. Kurumaji, M. Kriener, Y. Yamasaki, H. Sagayama, H. Nakao, K. Ohishi, K. Kakurai, Y. Taguchi, X. Yu, T.-H. Arima, and Y. Tokura, Nat. Commun. **10**, 5831 (2019).
[12] Y. Ōnuki, Y. Kaneko, D. Aoki, A. Nakamura, T. D. Matsuda, M. Nakashima, Y. Haga, and T. Takeuchi, J. Phys. Soc. Jpn. **91**, 065002 (2022).
[13] O. K. Andersen, Phys. Rev. B **12**, 3060 (1975).
[14] H. Yamauchi, D. P. Sari, I. Watanabe, Y. Yasui, L.-J. Chang, K. Kondo, T. U. Ito, M. Ishikado, M. Hagihara, M. D. Frontzek, S. Chi, J. A. Fernandez-Baca, J. S. Lord, A. Berlie, A. Kotani, S. Mori, and S.-i. Shamoto, Commun. Mater. **1**, 43 (2020).
[15] See Supplemental Material at http://link.aps.org/supplemental/10.1103/PhysRevMaterials.7.114402 for energy-dispersive x-ray analysis of bulk samples of Mn_3IrSi and Mn_3RhGe, dc susceptibility versus temperature data sets for Mn_3RhGe and Mn_3IrSi, and additional details of the magnetic structures of Mn_3IrSi and Mn_3RhGe and the mean-field calculations examining the incommensurate magnetic structure in Mn_3RhGe.
[16] J. F. Qian, A. K. Nayak, G. Kreiner, W. Schnelle, and C. Felser, J. Phys. D: Appl. Phys. **47**, 305001 (2014).
[17] L. C. Chapon, P. Manuel, P. G. Radaelli, C. Benson, L. Perrott, S. Ansell, N. J. Rhodes, D. Raspino, D. Duxbury, E. Spill, and J. Norris, Neutron News **22**, 22 (2011).
[18] J. Rodríguez-Carvajal, IUCr Commiss. Powder Diffract. Newslett. **26**, 12 (2001).
[19] V. Petříček, M. Henriques, and M. Dušek, Acta Cryst. **A77**, C175 (2021).
[20] R. W. Tyler, Phys. Rev. **44**, 776 (1933).
[21] D. Bloch, J. L. Feron, R. Georges, and I. S. Jacobs, J. Appl. Phys. **38**, 1474 (1967).
[22] M. S. Jagadeesh and M. S. Seehra, Phys. Rev. B **23**, 1185 (1981).
[23] B. J. Campbell, H. T. Stokes, J. M. Perez-Mato, and J. Rodríguez-Carvajal, Acta Cryst. **A78**, 99 (2022).
[24] J. M. Perez-Mato, J. L. Ribeiro, V. Petříček, and M. I. Aroyo, J. Phys.: Condens. Matter **24**, 163201 (2012).
[25] H. T. Stokes, D. M. Hatch, and B. J. Campbell, ISOTROPY software suite, iso.byu.edu.
[26] B. J. Campbell, H. T. Stokes, D. E. Tanner, and H. D. M., Acta Cryst. **39**, 607 (2006).
[27] L. D. Landau and E. M. Lifshitz, *Statistical Physics. Course of Theoretical Physics.* (Pergamon, Oxford, 1997).
[28] Y. Togawa, Y. Kousaka, K. Inoue, and J.-I. Kishine, J. Phys. Soc. Jpn. **85**, 112001 (2016).
[29] S. Mühlbauer, B. Binz, F. Jonietz, C. Pfleiderer, A. Rosch, A. Neubauer, R. Georgii, and P. Böni, Science **323**, 915 (2009).
[30] B. Canals and C. Lacroix, Phys. Rev. B **61**, 11251 (2000).
[31] J. A. M. Paddison, J. R. Stewart, P. Manuel, P. Courtois, G. J. McIntyre, B. D. Rainford, and A. L. Goodwin, Phys. Rev. Lett. **110**, 267207 (2013).
[32] A. Hall, P. Manuel, D. Khalyavin, F. Orlandi, D. Mayoh, L.-J. Chang, Y.-S. Chen, D. Jonas, M. Lees, and G. Balakrishnan, Neutron diffraction data for comparative study of the magnetism in Mn_3RhGe and related compound Mn_3IrSi [Data set] (2023), https://zenodo.org/records/10026585.